Super-stretchable Graphene Oxide Macroscopic Fibers with Outstanding Knotability Fabricated by Dry Film Scrolling

Rodolfo Cruz-Silva,[†] Aaron Morelos-Gomez,[‡] Hyung-ick Kim,[∞] Hong-kyu Jang,[¥] Ferdinando Tristan,[†] Sofia Vega-Diaz,[†] Lakshmy P. Rajukumar,[⊥,∥] Ana Laura Elías,[∥,#] Nestor Perea-Lopez,[∥,#] Jonghwan Suhr,[§,△] Morinobu Endo,[†,‡] and Mauricio Terrones[†,⊥,∥,#,¶,*]

[†]Research Center for Exotic Nanocarbons and [‡]Faculty of Engineering, Shinshu University, 4-17-1 Wakasato, Nagano 380-8553, Japan, [∞]Manufacturing Process Technology Innovation Center, Korean Institute of Industrial Technology, Jinju 660-805, South Korea, [¥]Composites Research Center, Korea Institute of Materials Science, Changwon 642-831, South Korea, [⊥]Department of Materials Science and Engineering, [∥]Center for 2-Dimensional and Layered Materials, [#]Department of Physics, and [¶]Department of Chemistry, The Pennsylvania State University, University Park, Pennsylvania 16802, United States, and [§]Center for Composite Materials, University of Delaware, Newark, Delaware 19716-3144, United States. [△]Present address: Department of Polymer Science & Engineering, Department of Energy Science, Sungkyunkwan University, Suwon 440-748, Korea.

ABSTRACT Graphene oxide (GO) has recently become an attractive building block for fabricating graphene-based functional materials. GO films and fibers have been prepared mainly by vacuum filtration and wet spinning. These materials exhibit relatively high Young's moduli but low toughness and a high tendency to tear or break. Here, we report an alternative method, using bar coating and drying of water/GO dispersions, for preparing large-area GO thin films (*e.g.*, 800−1200 cm^2 or larger) with an outstanding mechanical behavior and excellent tear resistance. These dried films were subsequently scrolled to prepare GO fibers with extremely large elongation to fracture (up to 76%), high toughness (up to 17 J/m^3), and attractive macroscopic properties, such as uniform circular cross section, smooth surface, and great knotability. This method is simple, and after thermal reduction of the GO material, it can render highly electrically conducting graphene-based fibers with values up to 416 S/cm at room temperature. In this context, GO fibers annealed at 2000 °C were also successfully used as electron field emitters operating at low turn on voltages of *ca.* 0.48 V/μm and high current densities (5.3 A/cm^2). Robust GO fibers and large-area films with fascinating architectures and outstanding mechanical and electrical properties were prepared with bar coating followed by dry film scrolling.

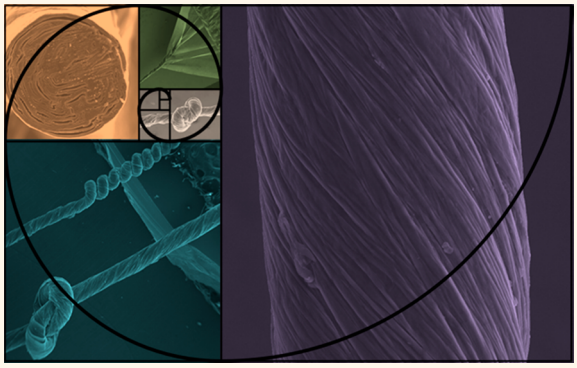

KEYWORDS: graphene paper · conductive fiber · bar coating · spinning · cast film · field emission

Graphene oxide (GO) films have attracted great attention because they can be reduced (thermally or chemically) into graphene and, furthermore, be prepared in bulk quantities (kilograms). Additionally, GO is water-dispersible, even in high concentrations, thus resulting in an environmentally friendly material.[1,2] GO can be regarded as a 2D material with extraordinary properties. Recently, films made of GO have shown outstanding separation capabilities.[3,4] GO has also been proposed as a high-performance structural material due to its exceptional mechanical behavior. For example, macroscopic fibers made of GO and reduced GO have been recently prepared by wet spinning.[5−14] These fibers show remarkable mechanical properties, such as high modulus and tensile strength[12] (20−25 GPa and 400−440 MPa, respectively) and, after reduction, good electrical conductivity[8] (400 S/cm). Unfortunately, these wet-spun fibers possess low toughness, rough surfaces, and highly irregular cross sections. These issues are important in terms of the fiber performance because the rough surface increases considerably the self-abrasion, while the irregular cross

* Address correspondence to mtterrones@shinshu-u.ac.jp, mut11@psu.edu.

Received for review February 24, 2014 and accepted May 5, 2014.

Published online May 05, 2014
10.1021/nn501098d

section of the fibers results in unwanted stress concentration under mechanical loadings, thus making them particularly susceptible to breaking. Although these wet-spun fibers could exhibit relatively high Young's modulus and high tensile strength, for the aforementioned reasons, they are found to be very brittle and easily breakable upon bending, twisting, or knotting, a clear disadvantage for various applications. Here we report a method based on a different approach which results in very tough GO fibers with outstanding mechanical performance. First, films of increased toughness were successfully made by bar coating water-based dispersions of GO followed by drying at room temperature. These films were subsequently scrolled into fibers displaying smooth surface, high toughness, outstanding ductility, and uniform circular cross sections. The fiber spinning process was carried out in dry state and could be used to easily prepare multifunctional GO nanocomposite fibers.

RESULTS AND DISCUSSION

We first prepared an aqueous dispersion of GO sheets (Figure 1a) based on a previously described method reported by Marcano *et al.*[15] The structural characterization (Raman, TGA, XPS, and XRD) of the produced GO are shown in Supporting Information Figure S1). This GO dispersion was then concentrated by centrifugation into a thick slurry (Figure 1b), which consists of *ca.* 0.8% wt of large GO single sheets (size distribution Figure S2) that were spread by bar coating on a PTFE plate (Figure 1c). Due to the liquid crystal structure (see Figure S3) and high viscosity of the dispersion, complete dewetting did not occur. The GO aqueous slurry was dried and carefully lifted off (Figure 1d) into large-area transparent and free-standing thin GO films. By using this simple technique, we were able to produce GO films with densities as low as 0.2 mg/cm^2 and areas as large as 800−1200 cm^2 (Figure S4), this area being limited only by the size of the PTFE plates available. These films are well-ordered, as previously reported,[16] and apparently resemble those prepared by vacuum filtration.[17] Nevertheless, due to the microscopic roughness of the PTFE surface and the large sheet size of the GO, these films developed a slightly wrinkled structure that confers additional ductility, where the wrinkles probably act as "springs" (Figure 1e), thus resulting in a great capability to deform without tearing, which is evident during the lift-off process and handling (see Supporting Information movie 1). Typical stress−strain curves of these films are shown in Figure S5, and the mechanical properties are summarized in Table S.I. Remarkably, these films routinely reveal deformations to failure between 2 and 6% of strain with a toughness of more than 2 MPa. Interestingly, in other GO films prepared by filtration, less than 1% of deformation was observed at break as well as low toughness values[18] (0.4−0.6 MPa).

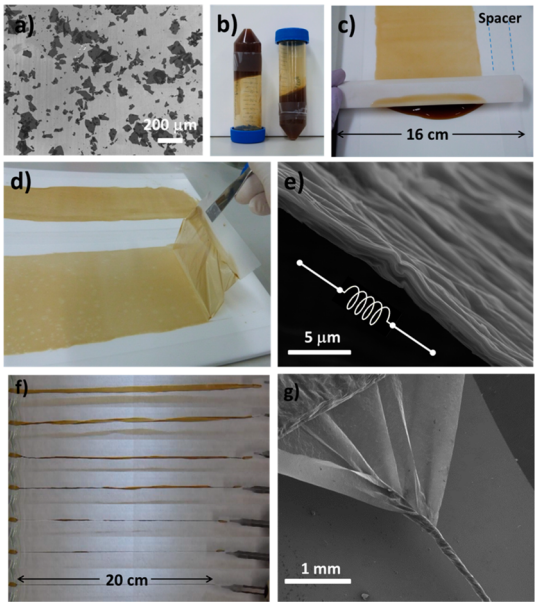

Figure 1. (a) SEM image of the large sheets of GO used as raw material in the preparation of GO films. (b) GO dispersion (0.87% wt) has a thick gel-like texture. (c) GO dispersion being spread over a PTFE plate using a PTFE bar and adhesive tape as spacer. (d) Free-standing thin (0.2 mg/cm^2) GO film is being lifted off. (e) SEM image of a 2.9 μm thick GO film showing the corrugated structure resulting from bar coating, which provides ductility through the kinks that might behave as springs. f) Fiber prepared by twisting (scrolling) a strip of GO films using an electric motor, showing different stages of the scrolling from top (beginning) to bottom (end). (g) SEM image of a thin GO film being scrolled into a fiber.

The Young's modulus observed in our films ranged from 1.4 and 1.7 GPa for films with thicknesses of 2.9 and 5.4 μm, respectively, and 5.7 GPa for the 0.74 μm thick sheets. These values are lower when compared to 32 GPa, a value reported by Dikin *et al.*,[17] but it is comparable to 5.8 GPa reported for GO paper measured at a low deformation stage.[19] In spite of the wrinkled structure, only the thinnest films (0.74 μm) displayed a self-reinforcing behavior upon elongation. The absence of self-reinforcing behavior in thicker films suggests that these films have lower sheet-to-sheet interactions, probably due to the lack of normal stress applied during filtration,[20] thus allowing sliding/slipping of the GO sheets under strain. Sheet-to-sheet interactions could be viewed as a type of physical cross-linking which is accountable for the stiffness and high modulus of the GO paper synthesized by filtration. Thus, the low sheet interaction might also contribute to the outstanding ductility shown in bar-coated GO films. While the 2.94 and 5.4 μm thick film exhibited similar mechanical properties and toughness, the 0.74 μm thick film had a remarkable behavior, by combining both the highest Young's modulus and highest toughness. This could be in part due to the higher contribution of an ordered skin, which contrasts to the disordered skin observed in films made by filtration. The thin skin seems to be stronger

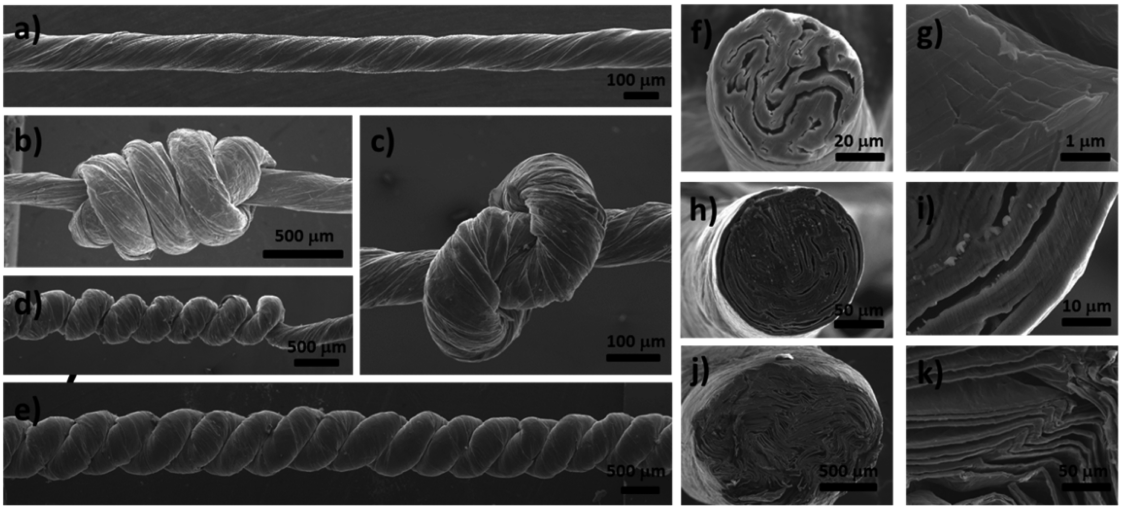

Figure 2. SEM images of GO fibers with different morphologies and knot architectures. (a) Typical dry-scrolled GO fiber; (b) quadruple overhand knot; (c) single knot; (d) self-coiled homochiral yarn; (e) neat two-ply yarn; (f) 60 μm diameter fiber made by mechanically scrolling a 0.74 μm thick GO sheet; (g) high-resolution image shows the layer-by-layer stacking within fibers; (h) cross section of a mechanically scrolled 150 μm diameter fiber; (i) zoom of the fiber cross section shown in (h); (j) cross section of a 1.1 mm diameter fiber made by manual scrolling; and (k) higher magnification image of (j) showing the formation of well-ordered areas of alternate stacks of GO sheets and voids.

and results from the drying process (schematized in Figure S6), and its contribution becomes important as the GO films become thinner.

Twisting or scrolling aligned carbon nanotube forests into fibers has become a relatively common process to prepare carbon nanotube fibers;[21,22,31] nevertheless, this intuitive approach has not been used to scroll GO films into fibers due to their tendency to tear and break. Recently, however, Cheng *et al.*[23] have reported the successful scrolling of a highly porous wet-spun graphene hydrogel fiber into a more compact GO fiber. Preparing GO fibers using dry processes is definitively attractive and opens up a more efficient alternative when compared to wet spinning. In this study, the outstanding toughness and ductility of GO bar-coated films allowed their spinning into pure GO fibers (see Supporting Information movie 2). We started by spinning a large diameter fiber using a relatively thick GO film (5.4 μm thick), and we were then able to progressively prepare small diameter fibers by using much thinner GO films. In this way, GO fibers with relatively smooth surface and circular cross section and diameter as small as 40 μm could be easily prepared. Figure 2a shows GO fibers with uniform diameter (circularity >0.95) and smooth surface. The preparation of thin and homogeneous GO films is essential since thick GO films result in the formation of defects, heterogeneities, and uneven fiber cross sections (see Figure S7a–d). Interestingly, free-standing GO films of 0.74 μm thickness showed a behavior not reported before for GO films. Figure S7e shows that these films could be bent and deformed dramatically without fracturing or experiencing structural failure, unlike thicker GO films prepared by filtration. Interestingly, 5.4 μm thick GO films made by bar coating and drying, as reported here, were fractured upon bending, thus indicating that only very thin GO films would result in mechanically tough and robust fibers (Figure S7f). Furthermore, the combination of the circular cross section and smooth surface allowed us to knot these fibers into a quadruple overhand knot (Figure 2b), which is impossible to make using wet-spun GO fibers because of their rough surface created during synthesis. Figure 2c shows a single knot that was tightly pulled, and no evidence of damage could be observed; when these fibers were twisted above their packing limit, they did not break but instead self-coiled into a single fiber with a secondary coil structure exhibiting the same chirality (Figure 2d). This morphology, although common in nanotube fibers,[21,31] has so far not been observed in pure GO fibers due to their tendency to break under torsional stress. In Figure 2e, we successfully made a two-ply yarn using two GO fibers. The robustness of these fibers upon bending and knotting, together with their low self-abrasion, makes them far superior to wet-spun GO fibers, which typically display very rough surface, high self-abrasion, and are prone to fracture, particularly at the knots. In order to study the internal structure and morphology of the fibers, we carried out cross-sectional cuts. The outer structure of GO fibers consisted of well-ordered and concentrically packed layers (see Figure 2f,h), whereas their central core consists of ordered sections of stacked GO films (Figure 2g,i), with void spaces between the planes, thus making them lighter in weight (as compared with solid GO fibers). The degree of layer packing was calculated from the diameter and the fiber density, and it was similar for fibers ranging from 1.6 mm to 300 μm in diameter (*ca.* 62% GO), whereas thinner fibers of *ca.* 110 μm diameter revealed

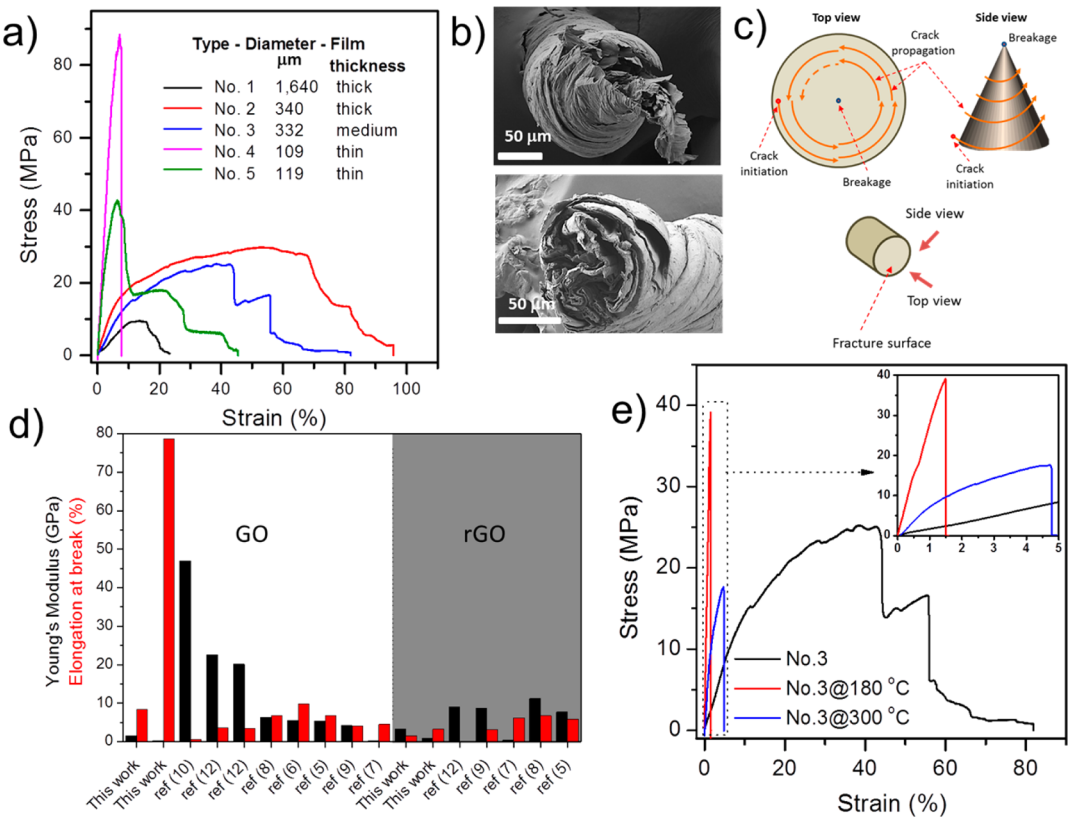

Figure 3. (a) Stress−strain curves for GO fibers. A progressive failure can be observed in most samples. (b) SEM images showing a typical fracture surface of GO fiber that shown progressive (top) or brittle (bottom) failure. (c) Proposed failure mechanism, showing the helical crack propagation. (d) Comparison of the elongation to break and Young's modulus of our dry-scrolled GO fibers with other reports using wet spinning methods. (e) Stress−strain curves for thermally reduced GO fibers compared to the pristine sample. The inset shows the low-strain region, where reduced GO fibers can be observed.

higher degree of packing (*ca.* 69%). These voids are also responsible for providing toughness to the fibers, thus allowing the GO sheets to slide when the fiber bends and avoiding the formation of fractures and their propagation. In natural fibers, voids are usually present and are responsible for increasing the fiber toughness by redistribution of the stress while decreasing the weight, such as the coconut and hemp fibers, which cross sections are shown in Figure S8.

We evaluated the mechanical properties of fibers prepared with GO films of various thicknesses ranging from 110 μm to 1.6 mm, and the results are summarized in Table S.II. Figure 3a shows a tensile stress−strain curve for several fibers where it is possible to notice their extreme elongation prior to failure. Under uniaxial deformation, our fibers first experience elastic deformation, most likely acting in part as coils, and elongate while reducing their diameter.[24] Therefore, there is a long plastic deformation when GO sheets within fibers slide with respect to one another, but later the fiber deforms irreversibly, until experiencing failure, which occurs progressively and in some samples (such as fiber type no. 3, in Figure 3a), the load could even rebuild. Few fibers of the narrowest diameter studied here showed brittle failure with significant enhanced Young's modulus and tensile strength. Therefore, the fibers were studied by SEM in order to understand the apparently different failure mechanism (Figure 3b). This image revealed that fibers that undergo progressive failure showed a cone-shaped fracture surface, caused by helical crack propagation, starting on the fiber surface and finishing on the fiber core (Figure 3c). Additional toughening occurs due to this energy-absorbing process, as well as film-to-film sliding during twisting due to the large deformation. In contrast, the fibers that experience a brittle fracture displayed a relatively flat fracture surface, which suggests that most of the fiber was participating in the load transfer. In agreement with this observation, the samples displaying brittle failure reached a tensile strength of 85 MPa, which is at least twice the stress experienced by fibers displaying a progressive failure. This brittle behavior was only observed in the thinnest fibers that were prepared and exhibited the highest sheet packing (69% solids). Effective tensile strength is higher due to fiber thinning at large uniaxial deformations.

Progressive failure is a characteristic displayed only in composites with secondary and tertiary structures, such as layered or reinforced carbon fiber composites. In our case, even though the fibers are made of pure GO, their structure is more complex than pure GO fibers made by wet spinning. Both fibers possess a

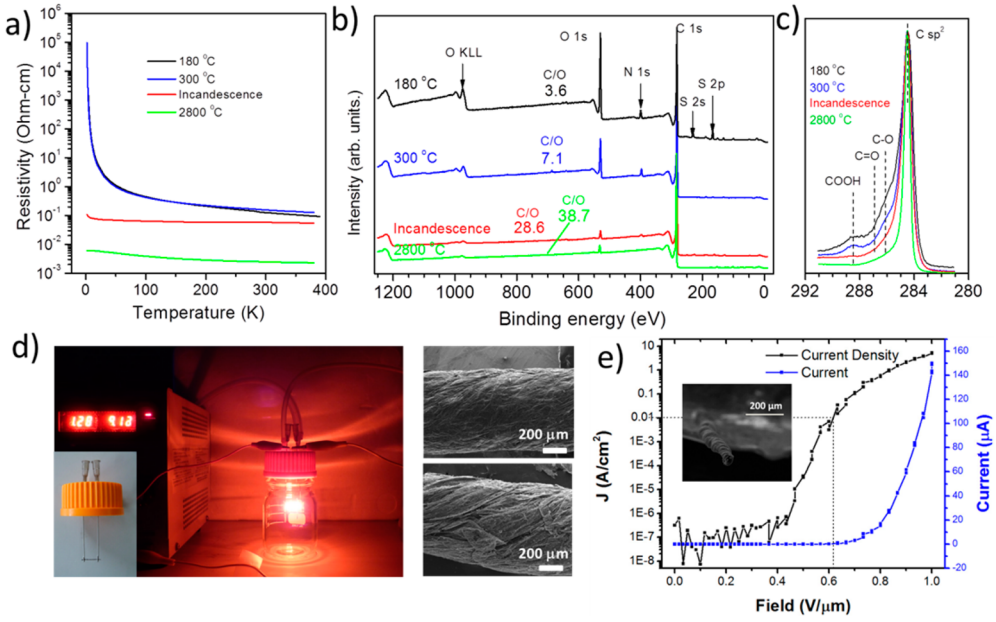

Figure 4. (a) Electrical conductivity behavior (resistivity *vs* temperature plots) of thermally reduced GO fibers. (b,c) Wide scan and core level XPS spectra, indicating the C/O evolution as a function of the thermal treatment of the fiber. (d) Set up used for the Joule effect heating of the rGO fiber. The inset depicts the fiber attached to stainless steel electrodes. The SEM image shows the surface of the fiber before (top) and after (bottom) the Joule heating experiment. (e) *I*–*E* curve for a thermally reduced GO fiber (shown in inset).

primary structure, which is represented by the packed face-to-face GO sheets. When twisting the film, the fibers acquire a secondary structure absent in wet-spun GO fibers, consisting of a helical spring-like structure that allows the fiber to strain up to 76% before observing a progressive failure. This value is almost 1 order of magnitude higher than the best values reported for pure GO fibers that were wet spun[6,8] and showed brittle failure (see Figure 3d and Supporting Information Table S.III).

The main interest in GO fibers is that they can be converted into electrically conducting reduced graphene oxide (rGO) fibers by chemical or thermal processes. In this context, we reduced these fibers by thermal treatment at 180 and 300 °C (see details in Methods). Figure 3e shows the comparison of the GO fiber before and after the thermal reduction. The reduction at 180 °C had a positive effect on the Young's modulus, by increasing its value more than 1 order of magnitude to 3.1 GPa. This phenomenon is due to the fiber densification and the chemical reduction of GO, which increases the sp^2/sp^3 hybridization ratio, thus providing stiffness to the individual sheets composing the fiber. However, when the fiber was further annealed to 300 °C, not only the Young's modulus decreases from 3.1 to 0.9 GPa but also the tensile strength value reduces from 39.2 to 14.1 MPa. The toughness of the rGO fibers was relatively low (0.3 MPa), and the mechanism of fracture turned brittle. We believe that by annealing above the deoxygenation temperature of GO (200 °C, as TGA shows in Figure S1b), rGO sheets lose most of the functional groups located at the edge of the sheets and consequently can no longer bond sheet-to-sheet by hydrogen bond forces; consequently, the stress transfer efficiency along the fiber decreases, weakening the fiber structure.

These rGO fibers were further annealed to 1050, 2000, and 2800 °C in order to study the electrical conductivity and electron field emission behavior (Figures 4a and 4e), as well as the chemical composition using XPS (Figure 4b,c) and Raman spectra (Figure S9). The two samples reduced at low temperature (180 and 300 °C) display a semiconducting behavior with a very drastic change in resistivity of up to 5 orders of magnitude in the region from 2 to 50 K, reaching a resistivity of 0.156 Ω·cm at 300 K, and despite having different C/O ratios, the electrical conductivity of both materials is similar. These values are slightly lower than reported values obtained by chemical reduction using hydroiodic acid[5,8,9] (HI). We then performed Joule annealing (Figure 4d) and calculated the temperature reached to be *ca.* 1480 °C (Figure S10). This thermal treatment was effective at removing the oxygen groups by changing the C/O ratio from 7.08 to 28, which resulted in a room temperature resistivity decrease to 0.057 Ω·cm. SEM images of the fiber (Figure 4d) before and after Joule heating shows that the outer layers of the graphene fiber were thermally evaporated. Further heat treatment at 2800 °C using a graphite furnace resulted in the complete deoxygenation of the fibers as indicated by the C/O ratio of 38.7 and a room temperature resistivity of 0.0024 Ω·cm (416 S/cm). The temperature resistance behavior of this fiber is

similar to that of graphite, thus suggesting the complete "graphitization" of the fiber, reaching the highest electrical conductivity reported for graphene-based fibers.[8] This conductivity value is still more than 2 orders of magnitude lower than those of crystalline carbon nanotube based fibers (ref 30 and references in Table S.IV). However, the recently developed graphene-based fibers belong to a different class of carbon materials, with different electrical properties, and more efforts must be made in order to improve their performance. In addition, the graphene-based fibers prepared in this work developed a supercoiled structure that has been observed previously in carbon nanotubes fibers,[21,22,31] and such highly coiled morphologies have not been reported hitherto for graphene-based fibers. Supercoiled structures usually result in a more complex mechanical behavior opening the possibilities to develop more elastic graphene-based fibers than those produced by wet spinning.

Since nanotubes have shown great potential as electron field emitters,[25] many carbon nanomaterials have also been studied as field emitters, and graphene has not been the exception.[26,27] We tested our rGO fibers treated at 2000 °C for field emission tests, and the *I*–*E* and electron emission current density (*J*) curves are shown in Figure 4e. The rGO fiber showed a turn-on field of 0.48 V/μm at 10 μA/cm^2, which is 1 order of magnitude lower than the 4.7 V/μm value for few-layer CVD-grown graphene[28] and 2.3 V/μm for reduced GO.[26] The threshold field (10 mA/cm^2) shown by the rGO film was only 0.62 V/μm, a value also lower than previous reports on reduced GO films prepared by electrophoretic deposition[26] (5.2 V/μm) or composite graphene films[27] (4 V/μm), but still larger than values reported for long and aligned multiwalled carbon nanotubes (MWNTs).[29] Current densities as high as 5.3 A/cm^2 were achieved at 1 V/μm electric fields, which is also a high value when compared to other reported graphene-like materials. The good field emission properties of our reduced graphene fibers are due to their intrinsic orientation of the GO sheets in the fiber, parallel to the fiber axis. For this reason, at the tip, there are many available graphene edges that act as effective emission sites, with high electrical conductivity and adequate atomic thickness, similarly to emitters made with tip-oxidized single-walled nanotubes.[32] Furthermore, the residual topological defects are expected to be located at the edges of the sheets,[33] thus providing localized states near the Fermi energy that facilitate the electron emission at low electric fields.

This simple method can also be applied to easily prepare hybrid macroscopic GO films and fibers by adding layers of different nanomaterials to the dried GO film. In particular, we have shown different examples of hybrid GO films and fibers with carbon nanotubes (double- and multiwalled), WS_2 layers, Ag nanowires (Ag NWs), and nylon nanofibers. Figure 5a shows

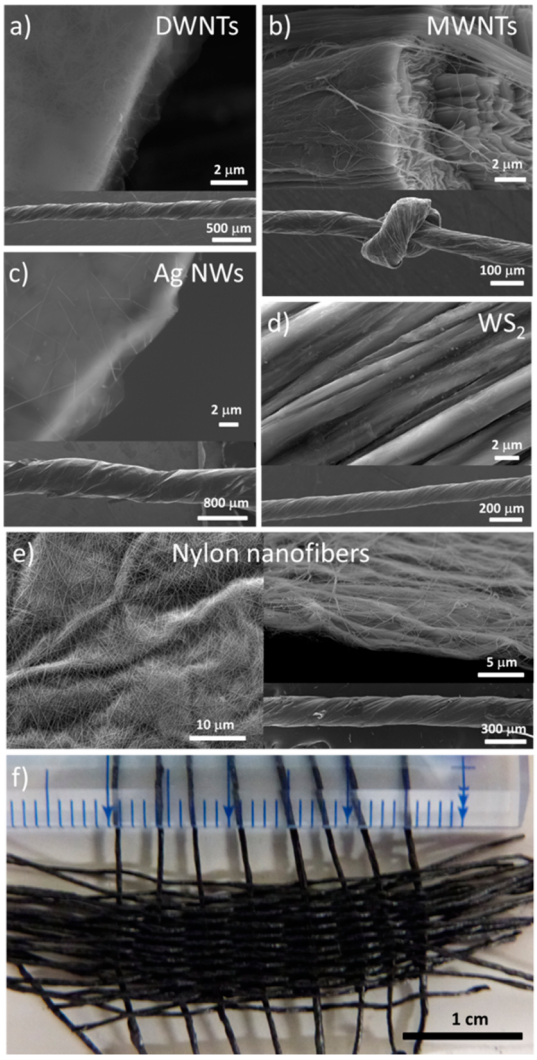

Figure 5. Hybrid films and macroscopic fibers made with graphene oxide films and (a) double walled carbon nanotubes, (b) multiwalled carbon nanotubes, (c) silver nanowires, (d) tungsten disulfide sheets, and (e) electrospun nylon nanofibers. (f) Fabric made using several GO macroscopic fibers.

a hybrid thin film consisting of a double-walled carbon nanotube (DWNT) layer on GO film that was prepared by drying an aqueous DWNT dispersion over the GO paper; the fiber was then fabricated by twisting the hybrid film. Figure 5b depicts a fiber generated by depositing dry MWNTs on the surface of the wet GO bar-coated dispersion. Other hybrid films containing Ag NWs and GO could also be produced by mixing aqueous dispersions of Ag NWs and GO followed by the same bar coating film preparation (Figure 5c); the silver nanowires can be seen embedded within the GO composite paper. Figure 5d shows a hybrid GO tungsten disulfide (WS_2) fiber made by dry rubbing WS_2 powder on the GO paper. The high-resolution image of the surface of the fiber shows the very thin WS_2 sheets coating the fiber. Alternatively, hybrid films made by electrospinning nylon nanofibers on top of a free-standing GO film could be produced, and the

subsequent twisting results in novel nylon nanofibers/GO composite macroscopic fibers (Figure 5e). Recently, the preparation of textiles based on GO fibers have gained attention.[8,12,14] We have also demonstrated that a GO-based fabric could be fabricated by weaving several macroscopic GO fibers (see Figure 5f). It is therefore clear that each of these hybrid materials represents a type of multifunctional GO fibers that could reveal unprecedented properties. Here, we have shown the proof of concept for relatively short fibers (up to 20 cm in length); however, unlike casting, bar coating is a method that can easily be adapted into a continuous process (see Supporting Information Figure S11) as it has been done before for polymers.[34] Similarly, continuous spinning procedures to make fibers are fully developed technologies for textiles and even carbon nanotube yarn production.[22,24]

CONCLUSIONS

Summarizing, large-area GO films were prepared in a simple way by bar coating and drying under environmental conditions. Their particular morphology provides them with great robustness and attractive mechanical properties. These films were converted into GO macroscopic fibers with a novel architecture by film scrolling. These fibers showed very high toughness, circular cross section, excellent knotability, and outstanding ductility. The method can be extended to prepare hybrid GO fibers containing different nanomaterials. The fibers were reduced by thermal treatment and Joule heating, achieving high electrical conductivity and were studied as electron field emitters. Their performance was enhanced by high-temperature treatment, achieving high current densities at low turn-on electric fields.

METHODS

Materials. Graphene flakes (product no. 332461-2.5KG, + 100 mesh, min. 75%) and hydrazine hydrate (64 wt %) were purchased from Sigma-Aldrich. Potassium permanganate ($KMnO_4$, 99%), sulfuric acid (H_2SO_4, 95 wt %), hydrogen peroxide (35 wt %), phosphoric acid (H_3PO_4, 85 wt %), and silver nitrate were reagent grade and purchased from Wako Chemical, Japan. All other reagents were of analytical grade or better.

Graphene Oxide Synthesis. Graphene oxide was prepared following a slight modification of the method reported by Marcano *et al.*[15] Briefly, 5 g of graphene was dispersed with magnetic stirring in a mixture of 200 mL of H_2SO_4 and 40 mL of H_3PO_4. Then 25 g of potassium permanganate was slowly added and dissolved, resulting in a green mixture. (Caution: permanganic acid should be handled carefully, avoiding mixing with organic solvents or heating above 55 °C at any time.) A thermometer was introduced to carefully monitor the temperature. The hot plate was magnetically stirred, and the temperature of the mixture reached *ca.* 40 °C. After 1 h of oxidation, the graphene exfoliated, and the mixture became a thick slurry, and magnetic stirring was interrupted, and a Teflon rod was used from this point to mix the slurry every 5 to 10 min. After 3.5 h of oxidation, the dark brown mixture was allowed to reach room temperature and then poured slowly in a mixture of 600 mL of cold water with 40 mL of 35% H_2O_2. This stage is accompanied by heating and vigorous bubbling. Finally, the GO bright yellow dispersion was left overnight to allow for complete neutralization of potassium permanganate.

Graphene Oxide Purification. The supernatant of the yellow GO dispersion was decanted, and the solid GO cake was dispersed in 1 L of 5 wt % H_2SO_4. During purification of GO, in order to preserve the large sheet size, magnetic stirring was avoided. Instead, a roller mixer was used. After redispersion, the GO dispersion was centrifuged a 4000 rpm for 5 min and the supernatant decanted. This step was repeated three times, but instead of acid, distilled water was used. While the acid is washed, the GO expands and the third time the GO pellet shows a two-layer structure. The bottom layer consists of larger unexfoliated particles of GO, and a top layer is a soft jelly-like dispersion that consists mainly of exfoliated graphene oxide sheets. This layer was collected with a spatula and dispersed in a large amount of water (4 L). Large unexfoliated particles that might be still present were removed by centrifugation at 4000 rpm for 3 min. The GO was washed by centrifugation, but from this point on, there is no solid pellet; instead, the GO dispersion separates into a brown dispersion at the bottom of the vial and a clear supernatant that can be decanted. Finally, it was concentrated into a slurry with pH 3.0−3.5 and 0.9% of solids by centrifugation at 6000 rpm for 3 h. A sample of GO gel was diluted by successive dilutions, and a drop was dried on a silicon wafer to study the sheet size distribution.

Graphene Oxide Film Preparation. Graphene oxide aqueous slurry was poured on a freshly polished (sand paper 2000 grit) Teflon block. Two or more layers of scotch tape (3M) were used as spacers to the desired thickness, and the slurry was spread by bar coating using a Teflon bar. The sample was dried overnight in the fume hood under forced air convection. The film was lifted off by using adhesive tape and careful peeling (see Figure 1 and Supporting Information movie 1).

Fiber Fabrication by Scrolling. Fibers were prepared by scrolling either mechanically (see Supporting Information movie 2, or manually). In order to have a successful scrolling, the film must be left to equilibrate at room temperature with 60% RH. Water has a plasticizer effect on GO, reducing its brittleness and increasing its toughness, thus tearing of the film is less likely to occur. After being scrolled, the fiber is very robust and flexible and can be handled in a wide range of temperatures or RH conditions. Hybrid DWNT/GO films were were prepared by drying a thin layer of polyelectrolyte-stabilized DWNT aqueous dispersion on top of a bar-coated GO dry film. Hybrid MWNT/GO films were prepared by attaching dried MWCNTs on top of wet bar-coated GO dispersion. Hybrid silver nanowires/GO films and fibers were prepared by mixing an aqueous dispersion of polyol-synthesized Ag NWs with a GO dispersion and following the same procedure used for making GO films and fibers. Tungsten sulfide (WS_2)/GO films and fibers were made by rubbing a free-standing GO films with tunsgten sulfide, then twisting it into a fiber. Hybrid nylon nanofibers/GO films were made by electrospinning a 9 wt % nylon-6,6 solution in formic acid on the surface of a free-standing GO film that was previously attached to rotary electrospinning equipment (0.2 mL/h, 15 kV electric field, and 10 cm tip to target distance). The fabric was made my manually knitting the GO fibers into a plain Dutch weave pattern.

Thermal Reduction. The fibers were attached to the glass. In order to avoid the fibers from untwisting during the heat treatment, a metallic weight (4.9 g for fibers with diameter up to 400 μm and 9.8 g for fibers with diameters larger than 400 μm) was attached to the lower end of the fiber. The temperature was increased from 80 to 180 °C at 20 °C increments each 24 h. The fiber was left at 180 °C for 24 h. The resulting fibers hardened and did not untwist after removing the weight. To further reduce the fibers at 300 °C, the fibers were introduced into a furnace using a quartz tube. Temperature was

increased from 180 to 300 °C at 20 °C increments each 20 min and left at 300 °C for 1 h. These fibers were stable and were subsequently heat treated at 1050, 2000, and 2800 °C for 30 min under argon atmosphere. Joule annealing was carried out in a homemade reactor filled with high-purity N_2. The incandescence emission was analyzed by using an oceanoptics 2000 spectrophotometer coupled to the reactor with optic fiber.

Measurement of Fiber Diameter. Cross sections were obtained by cutting the fibers using a focused ion beam system (SMI2050, SII, Japan). Fibers were examined by optical (Olympus BX-51 with a digital camera) and scanning electron microscopy SEM (JEOL JSM-6335 operating at 15 kV). Mechanical properties were measured using an Instron (model E300). Samples were attached to PET film mounting fixture using epoxy adhesive. Stress−strain curves were acquired at 50 μm/min. The force recorded by the load cell was used to derive the stress by using the cross-sectional areas.

Characterization. Thermogravimetric/differential thermal analysis (TGA/DTA) was carried out on TGA 8120 equipment under air flow (300 mL/min) and a 10 K/min heating rate using alumina powder as reference. Residual H_2SO_4 was analyzed using thermogravimetric analysis coupled with mass spectroscopy (TGA-MS) under a He/O_2 80/20 flow in a Rigaku ThermoMass photoequipment. X-ray photoelectron spectroscopy (XPS) analysis was carried out using the Al Kα line in an Axis-Ultra, Kratos, UK. The XPS analysis chamber was operated at 10^{-9} Torr, and the X-ray was focused in a 700 μm × 300 μm area, while the analyzer was set at 160 and 20 eV pass energy for the wide scan and narrow scan, respectively. Samples were grounded, and an electron gun was used to avoid charging during the measurements. Samples were referenced to the C 1s sp^2 peak at 284.5 eV. Semiquantitative elemental analysis was carried out using the C 1s, O 1s, S 2p, and P 2p from XPS, with relative sensitivity factors of (1, 1.8, 1.68, and 1.18, respectively). Raman spectroscopy was carried out in a Renishaw micro-Raman using the 633 nm lines. Fourier transformed infrared spectroscopic studies were carried out on Nicolet 6700 equipment in transmission mode. Field emission of the graphene fibers was measured at room temperature in the 10^{-6} Pa vacuum pressure. The emission current was monitored with a picoammeter (Keithley model 6485) connected in series with the emitter. The voltage was supplied by a DC high-voltage power supply and measured with a voltmeter. The fiber was fixed with silver paint to the cathode, and the anode was adjusted at a fixed position. The tip to anode separation was used to calculate the macroscopic electric field, $E = V/d$, and the current density $J = I/A$, where A is the transversal area of the fiber.

Electrical Conductivity Measurements. DC electrical conductivity was measured from 2 K to 379 K in a four-point probe configuration using a physical property measurement system from Quantum Design. Four copper electrodes were attached to the fiber using colloidal silver paint. The fiber was connected to the sample holder using copper wires.

Conflict of Interest: The authors declare no competing financial interest.

Acknowledgment. R.C.-S., F.T.-L., S.V.-D., M.T., and M.E. acknowledge support from the Research Center for Exotic Nanocarbons, Japan, Regional Innovation Strategy Program by the Excellence, JST. M.T. also acknowledges support from the Penn State Center for Nanoscale Science for seed grant on defects in 2-D Layered Materials (DMR-0820404) and from the U.S. Air Force Office of Scientific Research MURI Grant (FA9550-12-1-0035).

Supporting Information Available: Additional characterization is included in supplementary Figures S1−S11. Characteristics and mechanical properties of GO films, GO fibers, and a comparison of mechanical and electrical properties with reported values is provided in Tables S-I, S-II, S-III, and S-IV, respectively. The GO film lift-off process after bar coating followed by drying is provided as supporting video movie 1. The GO fiber preparation by mechanical spinning of GO films is shown in the supporting video movie 2. This material is available free of charge *via* the Internet at http://pubs.acs.org.

REFERENCES AND NOTES

1. Zhu, Y. W.; Murali, S.; Cai, W. W.; Li, X. S.; Suk, J. W.; Potts, J. R.; Ruoff, R. S. Graphene and Graphene Oxide: Synthesis, Properties, and Applications. *Adv. Mater.* **2010**, *22*, 3906–3924.
2. Zhu, Y.; James, D. K.; Tour, J. M. New Routes to Graphene, Graphene Oxide and Their Related Applications. *Adv. Mater.* **2012**, *24*, 4924–4955.
3. Li, H.; Song, Z.; Zhang, X.; Huang, Y.; Li, S.; Mao, Y.; Ploehn, H. J.; Bao, Y.; Yu, M. Ultrathin, Molecular-Sieving Graphene Oxide Membranes for Selective Hydrogen Separation. *Science* **2013**, *342*, 95–98.
4. Kim, H. W.; Yoon, H. W.; Yoon, S.-M.; Yoo, B. M.; Ahn, B. K.; Cho, Y. H.; Shin, H. J.; Yang, H.; Paik, U.; Kwon, S.; *et al.* Selective Gas Transport through Few-Layered Graphene and Graphene Oxide Membranes. *Science* **2013**, *342*, 91–95.
5. Xu, Z.; Gao, C. Graphene Chiral Liquid Crystals and Macroscopic Assembled Fibres. *Nat. Commun.* **2011**, *2*, 571.
6. Xu, Z.; Liu, Z.; Sun, H. Y.; Gao, C. Highly Electrically Conductive Ag-Doped Graphene Fibers as Stretchable Conductors. *Adv. Mater.* **2013**, *25*, 3249–3253.
7. Xu, Z.; Zhang, Y.; Li, P. G.; Gao, C. Strong, Conductive, Lightweight, Neat Graphene Aerogel Fibers with Aligned Pores. *ACS Nano* **2012**, *6*, 7103–7113.
8. Xu, Z.; Sun, H. Y.; Zhao, X. L.; Gao, C. Ultrastrong Fibers Assembled from Giant Graphene Oxide Sheets. *Adv. Mater.* **2013**, *25*, 188–193.
9. Cong, H.-P.; Ren, X.-C.; Wang, P.; Yu, S.-H. Wet-Spinning Assembly of Continuous, Neat, and Macroscopic Graphene Fibers. *Sci. Rep.* **2012**, *2*, 613.
10. Xiang, C.; Young, C. C.; Wang, X.; Yan, Z.; Hwang, C.-C.; Cerioti, G.; Lin, J.; Kono, J.; Pasquali, M.; Tour, J. M. Large Flake Graphene Oxide Fibers with Unconventional 100% Knot Efficiency and Highly Aligned Small Flake Graphene Oxide Fibers. *Adv. Mater.* **2013**, *25*, 4592–4597.
11. Shin, M. K.; Lee, B.; Kim, S. H.; Lee, J. A.; Spinks, G. M.; Gambhir, S.; Wallace, G. G.; Kozlov, M. E.; Baughman, R. H.; Kim, S. J. Synergistic Toughening of Composite Fibres by Self-Alignment of Reduced Graphene Oxide and Carbon Nanotubes. *Nat. Commun.* **2012**, *3*, 650.
12. Jalili, R.; Aboutalebi, S. H.; Esrafilzadeh, D.; Shepherd, R. L.; Chen, J.; Aminorroaya-Yamini, S.; Konstantinov, K.; Minett, A. I.; Razal, J. M.; Wallace, G. G. Scalable One-Step Wet-Spinning of Graphene Fibers and Yarns from Liquid Crystalline Dispersions of Graphene Oxide: Towards Multifunctional Textiles. *Adv. Funct. Mater.* **2013**, *23*, 5345–5354.
13. Sun, J.; Li, Y.; Peng, Q.; Hou, S.; Zou, D.; Shang, Y.; Li, Y.; Li, P.; Du, Q.; Wang, Z.; *et al.* Macroscopic, Flexible, High-Performance Graphene Ribbons. *ACS Nano* **2013**, *7*, 10225–10232.
14. Aboutalebi, S. H.; Jalili, R.; Esrafilzadeh, D.; Salari, M.; Gholamvand, Z.; Yamini, S. A.; Konstantinov, K.; Shepherd, R. L.; Chen, J.; Moulton, S. E.; *et al.* High-Performance Multifunctional Graphene Yarns: Toward Wearable All-Carbon Energy Storage Textiles. *ACS Nano* **2014**, *8*, 2456–2466.
15. Marcano, D. C.; Kosynkin, D. V.; Berlin, J. M.; Sinitskii, A.; Sun, Z. Z.; Slesarev, A.; Alemany, L. B.; Lu, W.; Tour, J. M. Improved Synthesis of Graphene Oxide. *ACS Nano* **2010**, *4*, 4806–4814.
16. Aboutalebi, S. H.; Gudarzi, M. M.; Zheng, Q. B.; Kim, J. K. Spontaneous Formation of Liquid Crystals in Ultralarge Graphene Oxide Dispersions. *Adv. Funct. Mater.* **2011**, *21*, 2978–2988.
17. Dikin, D. A.; Stankovich, S.; Zimney, E. J.; Piner, R. D.; Dommett, G. H. B.; Evmenenko, G.; Nguyen, S. T.; Ruoff, R. S. Preparation and Characterization of Graphene Oxide Paper. *Nature* **2007**, *448*, 457–460.
18. Gao, Y.; Liu, L. Q.; Zu, S. Z.; Peng, K.; Zhou, D.; Han, B. H.; Zhang, Z. The Effect of Interlayer Adhesion on the Mechanical Behaviors of Macroscopic Graphene Oxide Papers. *ACS Nano* **2011**, *5*, 2134–2141.
19. Park, S.; Lee, K. S.; Bozoklu, G.; Cai, W.; Nguyen, S. T.; Ruoff, R. S. Graphene Oxide Papers Modified by Divalent Ions—Enhancing Mechanical Properties *via* Chemical Cross-Linking. *ACS Nano* **2008**, *2*, 572–578.
20. Compton, O. C.; Cranford, S. W.; Putz, K. W.; An, Z.; Brinson, L. C.; Buehler, M. J.; Nguyen, S. T. Tuning the Mechanical

Properties of Graphene Oxide Paper and Its Associated Polymer Nanocomposites by Controlling Cooperative Intersheet Hydrogen Bonding. *ACS Nano* **2012**, *6*, 2008–2019.
21. Lima, M. D.; Li, N.; de Andrade, M. J.; Fang, S. L.; Oh, J.; Spinks, G. M.; Kozlov, M. E.; Haines, C. S.; Suh, D.; Foroughi, J.; *et al*. Electrically, Chemically, and Photonically Powered Torsional and Tensile Actuation of Hybrid Carbon Nanotube Yarn Muscles. *Science* **2012**, *338*, 928–932.
22. Li, Y. L.; Kinloch, I. A.; Windle, A. H. Direct Spinning of Carbon Nanotube Fibers from Chemical Vapor Deposition Synthesis. *Science* **2004**, *304*, 276–278.
23. Cheng, H.; Hu, Y.; Zhao, F.; Dong, Z.; Wang, Y.; Chen, N.; Zhang, Z.; Qu, L. Moisture-Activated Torsional Graphene-Fiber Motor. *Adv. Mater.* **2014**, DOI: 10.1002/adma.201305708.
24. Koziol, K.; Vilatela, J.; Moisala, A.; Motta, M.; Cunniff, P.; Sennett, M.; Windle, A. High-Performance Carbon Nanotube Fiber. *Science* **2007**, *318*, 1892–1895.
25. Deheer, W. A.; Chatelain, A.; Ugarte, D. A Carbon Nanotube Field-Emission Electron Source. *Science* **1995**, *270*, 1179–1180.
26. Wu, Z. S.; Pei, S. F.; Ren, W. C.; Tang, D. M.; Gao, L. B.; Liu, B. L.; Li, F.; Liu, C.; Cheng, H. M. Field Emission of Single-Layer Graphene Films Prepared by Electrophoretic Deposition. *Adv. Mater.* **2009**, *21*, 1756–1760.
27. Eda, G.; Unalan, H. E.; Rupesinghe, N.; Amaratunga, G. A. J.; Chhowalla, M. Field Emission from Graphene Based Composite Thin Films. *Appl. Phys. Lett.* **2008**, *93*, 233502.
28. Wang, J. J.; Zhu, M. Y.; Outlaw, R. A.; Zhao, X.; Manos, D. M.; Holloway, B. C.; Mammana, V. P. Free-Standing Subnanometer Graphite Sheets. *Appl. Phys. Lett.* **2004**, *85*, 1265–1267.
29. Perea-Lopez, N.; Rebollo-Plata, B.; Antonio Briones-Leon, J.; Morelos-Gomez, A.; Hernandez-Cruz, D.; Hirata, G. A.; Meunier, V.; Botello-Mendez, A. R.; Charlier, J.-C.; Maruyama, B.; *et al.* Millimeter-Long Carbon Nanotubes: Outstanding Electron-Emitting Sources. *ACS Nano* **2011**, *5*, 5072–5077.
30. Behabtu, N.; Young, C. C.; Tsentalovich, D. E.; Kleinerman, O.; Wang, X.; Ma, A. W. K.; Bengio, E. A.; Waarbeek, R. F.; Jong, J. J.; Hoogerwerf, R. E.; *et al.* Strong, Light, Multifunctional Fibers of Carbon Nanotubes with Ultrahigh Conductivity. *Science* **2013**, *339*, 182–186.
31. Shang, Y.; He, X.; Li, Y.; Zhang, L.; Li, Z.; Ji, C.; Shi, E.; Li, P.; Zhu, K.; Peng, Q.; *et al.* Super-stretchable Spring-like Carbon Nanotube Ropes. *Adv. Mater.* **2012**, *24*, 2896–2900.
32. Rinzler, A. G.; Hafner, J. H.; Nikolaev, P.; Lou, L.; Kim, S. G.; Tomanek, D.; Nordlander, P.; Colbert, D. T.; Smalley, R. E. Unraveling Nanotubes—Field-Emission from an Atomic Wire. *Science* **1995**, *269*, 1550–1553.
33. Meyer, J. C.; Kisielowski, C.; Erni, R.; Rossell, M. D.; Crommie, M. F.; Zettl, A. Direct Imaging of Lattice Atoms and Topological Defects in Graphene Membranes. *Nano Lett.* **2008**, *8*, 3582–3586.
34. Ouyang, J. Y.; Guo, T. F.; Yang, Y.; Higuchi, H.; Yoshioka, M.; Nagatsuka, T. High-Performance, Flexible Polymer Light-Emitting Diodes Fabricated by a Continuous Polymer Coating Process. *Adv. Mater.* **2002**, *14*, 915–918.